

Nanoscale

Accepted Manuscript



This is an *Accepted Manuscript*, which has been through the Royal Society of Chemistry peer review process and has been accepted for publication.

Accepted Manuscripts are published online shortly after acceptance, before technical editing, formatting and proof reading. Using this free service, authors can make their results available to the community, in citable form, before we publish the edited article. We will replace this *Accepted Manuscript* with the edited and formatted *Advance Article* as soon as it is available.

You can find more information about *Accepted Manuscripts* in the [Information for Authors](#).

Please note that technical editing may introduce minor changes to the text and/or graphics, which may alter content. The journal's standard [Terms & Conditions](#) and the [Ethical guidelines](#) still apply. In no event shall the Royal Society of Chemistry be held responsible for any errors or omissions in this *Accepted Manuscript* or any consequences arising from the use of any information it contains.

COMMUNICATION

Design and Assembly of Supramolecular Dual-modality Nanoprobes

Cite this: DOI: 10.1039/x0xx00000x

Shuang Liu,^a Pengcheng Zhang,^a Sangeeta Ray Banerjee,^b Jiadi Xu,^c Martin Pomper,^b and Honggang Cui^{*a,d}

Received 00th January 2012,
Accepted 00th January 2012

DOI: 10.1039/x0xx00000x

www.rsc.org/

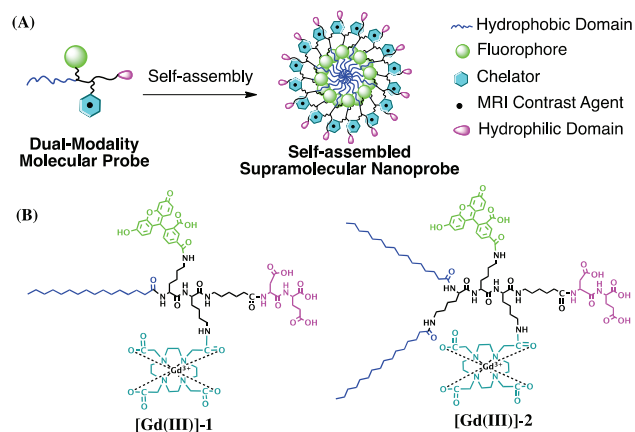
We report the design and synthesis of self-assembling dual-modality molecular probes containing both a fluorophore for optical imaging and a metal ion chelator for imaging with MRI or radionuclide methods. These molecular probes can spontaneously associate into spherical nanoparticles under physiological conditions. We demonstrate the use of these supramolecular nanoprobes for live-cell optical imaging, as well as their potential use as MRI contrast agents after complexation with gadolinium. Our results suggest that self-assembly into supramolecular nanoprobes presents an effective means to enhance and tune the relaxivities of molecular probes.

Self-assembly of a simple molecular building unit can yield complex supramolecular architectures with new functions that the individual unit does not carry.¹ This strategy has been used to create a plethora of interesting nanoscopic and microscopic morphologies from block copolymers,²⁻⁴ small molecular amphiphiles,^{1, 5, 6} peptides,⁷⁻¹² proteins,¹³ and DNA.^{14, 15} The specific control over size, shape, surface chemistry, and degradation kinetics enables supramolecular nanostructures the unique capacity for use as carriers to deliver therapeutic or diagnostic agents.¹⁶⁻¹⁹ In this carrier-cargo approach, the self-assembling units are typically biocompatible and biodegradable but biologically inert molecules that do not possess any function beyond ensuring the specific delivery and controlled release of the functional units. On the other hand, the functional molecules to be delivered, e.g. drugs, or molecular probes, are not expected to contribute to the self-assembly process. Here we report the use of dual-modality molecular imaging probes to directly create self-assembling supramolecular nanoprobes with the capacity for both optical and magnetic resonance (MR) imaging.

Nanoparticles that have been used to image cancers have several advantages over individual molecular probes.²⁰⁻²⁴ First, nanoparticles can be accumulated at tumor sites through the enhanced permeability and retention (EPR) effect,²⁵ which consequently increases the signal-to-noise ratio.²⁶ Second, nanoparticles can generate signal amplification and enhance sensitivity.²⁷ Third, nanoparticles can be a platform for multiple functions, with components either incorporated

within or through surface modification, which could enable superior pharmacokinetics and/or active targeting.^{28, 29}

Scheme 1. (A) Rational design of self-assembling, dual-modality molecular probes containing four essential elements: a hydrophobic domain to promote self-assembly in aqueous environments, a fluorophore for optical imaging, a chelator to enable complexation with metals, such as gadolinium (Gd) for MR contrast, and a hydrophilic headgroup. These amphiphilic molecules are designed to self-assemble into spherical nanoparticles. (B) Chemical structures of the two probes used in the study: [Gd(III)]-1 and [Gd(III)]-2.



Here we report the design and synthesis of supramolecular dual-modality nanoprobes by self-assembly of amphiphilic building blocks containing a fluorophore and a metal ion chelator. In the context of molecular imaging, each imaging modality offers its own advantages and disadvantages in terms of sensitivity, spatial resolution and depth of tissue penetration.^{30, 31} Optical imaging with the fluorescent aspect of the probe has high sensitivity, while MR is widely used clinically for detection and therapeutic monitoring of cancer.³² Multi-modality probes could provide complementary information, enabling both pre-operative staging and real-time, image-guided surgery for the management of cancer.³³⁻³⁵ In this work, we demonstrated live-cell fluorescence imaging of self-

assembled nanoprobes in KB-3-1 human cervical cancer cells and assessed their feasibility to serve as contrast agents for MR imaging.

The self-assembly illustration of two dual-modality amphiphilic probes, [Gd(III)]-1 and [Gd(III)]-2, and their molecular structures are shown in Scheme 1. The amphiphilic nature of probes **1** and **2** stems from incorporation of both hydrophobic n-alkyl chains on the N-termini and the hydrophilic domain on the C-termini. The fluorophore 5-carboxyfluorescein (5-FAM) and MR contrast moiety - gadolinium complex of 1,4,7,10-tetraazacyclododecane-1,4,7,10-tetraacetic acid (Gd-DOTA) - were introduced through reaction with a lysine residue present on the probe and the activated ester of the corresponding imaging agent. The amphiphilicity of these two probes is expected to enable them to spontaneously self-assemble into nanostructures in an aqueous environment, forming core-shell micelles with a hydrophobic core and hydrophilic moieties outside. The negatively charged dipeptide and the flexible linker on the C-terminal also improve solubility, preventing aggregation and non-specific association with proteins and cells.

Probes **1** and **2** were synthesized using a standard Fmoc-based solid phase peptide synthesis protocol using selectively protected lysine residues for functional group incorporation. (Details can be found in Figure S1 in supporting information [SI]). The chelation of probes **1** and **2** with Gd³⁺ was conducted in water at pH 10 to 11 and at 80 °C for 2 hours in the presence of an excess of GdCl₃.^{36, 37} Gadolinium complexes were purified using reverse-phase HPLC to remove excess gadolinium salt, and the products were characterized using mass spectrometry and analytical HPLC (Figure S2). Due to the coordination of Gd³⁺ with carboxylic acid groups on the chelator, DOTA, the negative charges on DOTA were partially neutralized to ensure longer retention times on HPLC of the complexes compared to the un-complexed substrate.

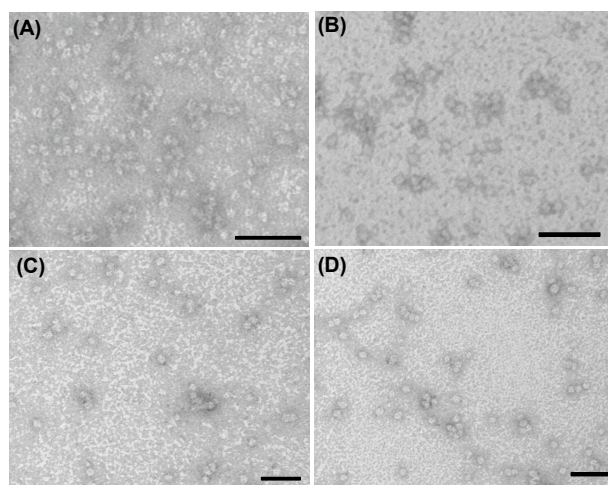


Figure 1. TEM images of self-assembled probes **1** (A), **2** (B), [Gd(III)]-1 (C) and [Gd(III)]-2 (D) at 500 μ M in PBS at pH 7.4. TEM samples stained using a 2 wt% uranyl acetate aqueous solution to enhance imaging contrast. Scale bars are 50 nm.

Transmission electron microscopy (TEM) was used to characterize the morphology of the self-assembled nanostructures in PBS at pH 7.4. Representative TEM images of **1** and **2** and their gadolinium complexes [Gd(III)]-1 and [Gd(III)]-2 at 500 μ M in PBS are shown in Figure 1. The dominant features are uniformly distributed nanospheres with average diameters of 7.8 ± 1.2 nm, 8.2 ± 1.0 nm, 10.9 ± 1.9 nm and 10.7 ± 1.4 nm for **1**, **2**, [Gd(III)]-1 and [Gd(III)]-2, respectively. The amphiphilic nature of these molecules suggests that the nanospheres observed in the TEM images are likely

core-shell micelles. The diameters of **1** and **2** are approximately twice those of their respective extended chain lengths, which are 4.7 and 5.0 nm, respectively. The diameter of nanospheres formed from **2** is slightly larger than that of **1** possibly due to the extra lysine residue in **2**. The difference of micelle sizes after complexation likely results from a change in ionic charge status. Upon complexation, DOTA is partially neutralized and thus the repulsion between the headgroups would be reduced, so that more amphiphilic molecules can pack to fit into a spherical shape.³⁸ It is possible that at much higher concentrations other morphologies such as cylindrical micelles could be accessed as a result of minimizing system free energy to achieve an optimal headgroup area.

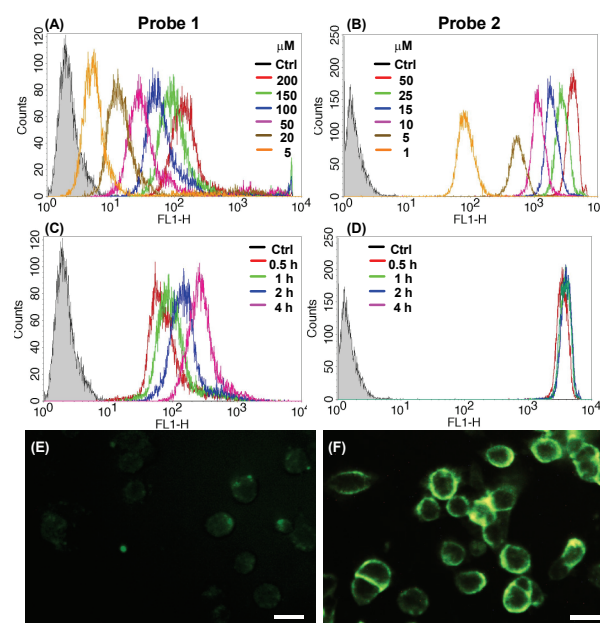


Figure 2. Representative flow cytometry histograms of KB-3-1 cells incubated with **1** and **2** to demonstrate concentration and time dependence. (A) Probe **1** (0-200 μ M) and (B) probe **2** (0-50 μ M) for 2 hours incubation. (C) Probe **1** (200 μ M) and (D) probe **2** (50 μ M) for 0.5, 1, 2 and 4 hours incubation. Representative fluorescent images of KB-3-1 cells after incubation with probe **1** (200 μ M) (E) and probe **2** (50 μ M) (F) for 2 hours. Scale bars are 20 μ m.

Cellular uptake studies were carried out to evaluate the feasibility of live-cell fluorescent imaging using KB-3-1 human cervical cancer cells incubated with probes **1** and **2**. Flow cytometry histograms indicate that cellular uptake of both probes was time and concentration dependent (Figure 2 (A) to (D)). The geometric mean of the signal intensity of **1** increased with sample concentration and incubation time, while for **2**, the signal intensity of cells reached a plateau after one hour and slightly decreased at longer incubation times and at higher sample concentrations (Figures S3 and S4). That decrease in fluorescence intensity may be due to fluorescence quenching after signal saturation upon the highly efficient cellular uptake of **2**. Fluorescent images of KB-3-1 cells after 2 hours of incubation with **1** (200 μ M) and **2** (50 μ M), with concentrations higher than their respective critical micelle concentrations (CMC) (*vide infra*), are shown in Figure 2 (E) and (F). The images indicate that the insertion of **2** into cell membranes is much more efficient than that of **1**, which was quantified *via* flow cytometry (Figure S5). Probe **2**, although studied at a lower concentration of 50 μ M, showed approximately 25-fold higher cellular uptake than **1** when studied at the higher concentration of 200 μ M. It should be noted that although

the concentrations of **1** and **2** used in these experiments were well above their respective CMC values, the solutions actually comprised a mixture of monomers with assembled micelles due to the dynamic nature of supramolecular assemblies. The dramatic difference in cellular uptake efficiency suggests that it is the monomer that draws the contrast in cell membrane accumulation and cellular internalization. Since both molecules are expected to be negatively charged under physiological conditions, cellular uptake should occur primarily by virtue of the hydrophobic alkyl chains, which have previously been used to modify the N-terminal of cell penetrating peptides in gene and drug delivery systems.³⁹⁻⁴² Therefore, it is reasonable that, with two alkyl chains on the N-terminal, **2** demonstrated higher cellular uptake than **1**. Confocal imaging (Figure S6) showed that **1** had entered cytosol, while **2** was mainly membrane-bound. Cytotoxicity studies of **1** and **2** were carried out using sulforhodamine B (SRB) staining.⁴³ As shown in Figure S7, almost no effects on cell viability were observed at concentrations up to 200 μM for **1** and 50 μM for **2** after incubation for 20 hours.

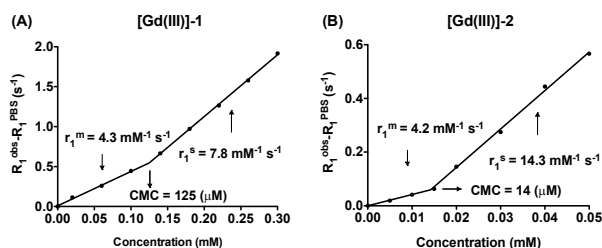


Figure 3. The plots of the reciprocals of T_1 relaxation time versus concentrations of **[Gd(III)]-1** (A) and **[Gd(III)]-2** (B) in PBS at pH 7.4 (25°C, 1 T). Longitudinal relaxivities r_1 were determined from the slope of the linear fits. The CMC of each probe was calculated based on relaxivities of monomer (r_1^m) and self-assembled nanoprobe (r_1^s).

Proton T_1 relaxation times were measured to study the relaxivities of the metallated versions of **1** and **2**. MRI of different concentrated solutions of **[Gd(III)]-1** and **[Gd(III)]-2** in PBS at pH 7.4 were performed on an Aspect M2 1T MRI scanner (Shoham, Israel) at room temperature. A standard inversion recovery sequence was used for the T_1 measurements. MR images for 13 and 10 different values of TI (time of inversion), ranging from 15 to 4,500 ms and 50 to 6,000 ms, were acquired for **[Gd(III)]-1** and **[Gd(III)]-2** respectively. As shown in Figures 3 (A) and (B), enhancement of relaxation rates (s^{-1}) over PBS is plotted against probe concentrations (mM). Relaxivities of monomer (r_1^m) and self-assembled nanoprobe (r_1^s) were determined from the slopes of linear fits. The CMCs were calculated based on two relaxivities, as described in SI, and 125 and 14 μM for **[Gd(III)]-1** and **[Gd(III)]-2** were obtained, respectively. When probe concentration fell below the CMC, the contribution to enhancement of the relaxation rate was mainly from non-assembled, monomeric molecular contrast agent. As individual molecules, the nature of **[Gd(III)]-1** and **[Gd(III)]-2** were similar, therefore, measured monomer relaxivity r_1^m of 4.3 and 4.2 $\text{mM}^{-1} \text{s}^{-1}$ for **[Gd(III)]-1** and **[Gd(III)]-2** were similar and comparable to those of other single molecular Gd-DOTA contrast agents reported, ranging from 3.5 to 4.8 $\text{mM}^{-1} \text{s}^{-1}$.⁴⁴

We found that the self-assembly of molecular contrast agents into supramolecular nanoprobe could significantly enhance the water proton relaxation rates. Micelle relaxivity r_1^s of 7.8 and 14.3 $\text{mM}^{-1} \text{s}^{-1}$ were obtained for **[Gd(III)]-1** and **[Gd(III)]-2**, respectively. Given their supramolecular nature, these self-assembled nanoprobe are in a dynamic equilibrium with the monomeric molecular contrast agents (monomers), but the monomer concentration would remain

constant at concentrations above the CMC.³⁸ The relaxivity of self-assembled micelles r_1^s measured above the CMC represents the relaxivity of the self-assembled nanostructures.⁴⁵ **[Gd(III)]-2** exhibited a greater increase in micelle relaxivity over monomer relaxivity than that of **[Gd(III)]-1**. This difference can be well explained by the denser packing of **[Gd(III)]-2** in the micellar state because it contains two hydrophobic alkyl tails, which led to a larger aggregation number and a higher total mass for **[Gd(III)]-2** micelles than that of **[Gd(III)]-1** micelles. The higher molar mass of micelles of **[Gd(III)]-2** slows the micelle rotational correlation time greater than for **[Gd(III)]-1**, which is known to increase the relaxivity of contrast agents.⁴⁶⁻⁴⁸ These results demonstrate that higher relaxivity can be achieved *via* self-assembly of nanoprobe to serve as MR contrast agents that are superior to the individual molecular probes. This increase in relaxivity can be engineered through careful design of the components of the self-assembling nanostructures.

The CMCs of **1** and **2** were also determined through fluorescence measurements. For both **1** and **2**, maximum emission fluorescence intensities increased approximately linearly with increasing concentrations initially and then decreased when the concentrations increased further (Figure S8). Transition of emission maximum occurred at concentrations above 130 μM and 15 μM for **1** and **2**, respectively, consistent with the CMCs measured from the aforementioned MR studies. Those transitions can be attributed to the formation of self-assembled nanostructures. When monomers self-assemble into micelles, fluorophore is packed within and partially quenched and the fluorescence signal plateaus with increasing concentration. The decrease of fluorescence signal was due to both the inner filter effects at high concentrations and the scattering from the increased number of micelles. In addition, peak positions of emission spectra of both probes exhibited red shifts with increasing concentration, and the shifts occurred to a greater extent above the CMC, indicating the local environmental change of the 5-FAM fluorophore. The CMC value of **2** was lower than that of **1**, simply because **2** is more hydrophobic, which can drive self-assembly at lower concentrations and also yield more stable supramolecular structures in an aqueous environment.

Conclusions

In summary, we report the synthesis of two amphiphilic dual-modality nanoprobe, each containing a fluorophore and a Gd-DOTA complex, which self-assemble into supramolecular nanostructures. Live-cell imaging studies suggest that these nanoprobe can effectively label cells with the assistance of their incorporated alkyl chains. The negatively charged surface of the resultant micelles causes no cytotoxicity at concentrations higher than the CMC for either nanoprobe. Self-assembly of the probes into nanostructures increased probe relaxivity, potentially providing superior contrast agents to conventional, unimolecular probes. All of these properties are controlled by design rules incorporated into the component building blocks, e.g., with two n-alkyl chains, **2** has a lower CMC, more stable structure, more efficient cellular uptake and a higher increase in relaxivity than **1**. We have shown that multi-modality probes can be designed to self-assemble into supramolecular nanostructures that have imaging properties superior to those of the independent components. Synthesis of nanoprobe with different sizes, shapes and surface modifications as well as *in vivo* evaluation of the resulting constructs are under way. And clearly, since supramolecular assemblies are a function of the assembly conditions, their stability in circulation and responsiveness to environmental changes would pose a great challenge in the fundamental design of supramolecular nanoprobe.

Notes and references

^a Department of Chemical and Biomolecular Engineering, Johns Hopkins University, 3400 N. Charles Street, Baltimore, MD 21218, United States.

^b The Russell H. Morgan Department of Radiology and Radiological Science, Johns Hopkins University 1550 Orleans Street, 492 CRB II, Baltimore, MD 21231, United States.

^c F.M. Kirby Research Center for Functional Brain Imaging, Kennedy Krieger Institute, Baltimore, MD 21205, United States.

^d Department of Oncology and Sidney Kimmel Comprehensive Cancer Center, Johns Hopkins University School of Medicine, Baltimore, Maryland 21205, United States

*Email: hcui6@jhu.edu

† Electronic Supplementary Information (ESI) available: [Experimental methods, materials, synthesis schemes, sample characterization, fluorescence measurements, cellular uptake and MRI experimental details]. See DOI: 10.1039/c000000x/

Acknowledgements

We thank the National Science Foundation (DMR 1255281) and W.W. Smith Charitable Trust for support of the project. We thank Dr. Michael McMahon in the Radiology Department, Johns Hopkins University for helpful discussion on the MRI studies.

References

1. T. Aida, E. W. Meijer and S. I. Stupp, *Science*, 2012, **335**, 813-817.
2. T. Gadt, N. S. Jeong, G. Cambridge, M. A. Winnik and I. Manners, *Nature Materials*, 2009, **8**, 144-150.
3. F. S. Bates, M. A. Hillmyer, T. P. Lodge, C. M. Bates, K. T. Delaney and G. H. Fredrickson, *Science*, 2012, **336**, 434-440.
4. H. Cui, Z. Chen, S. Zhong, K. L. Wooley and D. J. Pochan, *Science*, 2007, **317**, 647-650.
5. Y. Kuang, J. Shi, J. Li, D. Yuan, K. A. Alberti, Q. Xu and B. Xu, *Angewandte Chemie-International Edition*, 2014, **53**, 8104-8107.
6. R. Lin and H. Cui, *Current Opinion in Chemical Engineering*, 2015, **7**, 75-83.
7. B. E. I. Ramakers, J. C. M. van Hest and D. Lowik, *Chemical Society Reviews*, 2014, **43**, 2743-2756.
8. A. Trent, R. Marullo, B. Lin, M. Black and M. Tirrell, *Soft Matter*, 2011, **7**, 9572.
9. H. Cui, M. J. Webber and S. I. Stupp, *Biopolymers*, 2010, **94**, 1-18.
10. S. Sathaye, H. Zhang, C. Sonmez, J. P. Schneider, C. M. MacDermaid, C. D. Von Bargen, J. G. Saven and D. J. Pochan, *Biomacromolecules*, 2014, **15**, 3891-3900.
11. V. A. Kumar, N. L. Taylor, S. Shi, B. K. Wang, A. A. Jalan, M. K. Kang, N. C. Wickremasinghe and J. D. Hartgerink, *Acs Nano*, 2015, **9**, 860-868.
12. R. A. Pires, Y. M. Abul-Haija, D. S. Costa, R. Novoa-Carballal, R. L. Reis, R. V. Ulijn and I. Pashkuleva, *Journal of the American Chemical Society*, 2015, **137**, 576-579.
13. J. W. Kelly, *Current Opinion in Structural Biology*, 1998, **8**, 101-106.
14. P. W. K. Rothmund, *Nature*, 2006, **440**, 297-302.
15. T. R. Pearce and E. Kokkoli, *Soft Matter*, 2015, **11**, 109-117.
16. Y. Bae, S. Fukushima, A. Harada and K. Kataoka, *Angewandte Chemie-International Edition*, 2003, **42**, 4640-4643.
17. R. Haag, *Angewandte Chemie-International Edition*, 2004, **43**, 278-282.
18. A. T. Preslar, G. Parigi, M. T. McClendon, S. S. Sefick, T. J. Moyer, C. R. Haney, E. A. Waters, K. W. MacRenaris, C. Luchinat, S. I. Stupp and T. J. Meade, *Acs Nano*, 2014, **8**, 7325-7332.
19. C. M. J. Hu, R. H. Fang, B. T. Luk and L. F. Zhang, *Nature Nanotechnology*, 2013, **8**, 933-938.
20. W. B. Cai and X. Y. Chen, *Small*, 2007, **3**, 1840-1854.
21. M. L. Schipper, G. Iyer, A. L. Koh, Z. Cheng, Y. Ebenstein, A. Aharoni, S. Keren, L. A. Bentolila, J. Q. Li, J. H. Rao, X. Y. Chen, U. Banin, A. M. Wu, R. Sinclair, S. Weiss and S. S. Gambhir, *Small*, 2009, **5**, 126-134.
22. S. Chapman, M. Dobrovolskaia, K. Farahani, A. Goodwin, A. Joshi, H. Lee, T. Meade, M. Pomper, K. Ptak, J. Rao, R. Singh, S. Sridhar, S. Stern, A. Wang, J. B. Weaver, G. Woloschak and L. Yang, *Nano today*, 2013, **8**, 454-460.
23. P. Zhang, A. G. Cheetham, L. L. Lock, Y. Li and H. Cui, *Current opinion in biotechnology*, 2015, **34C**, 171-179.
24. C. M. J. Hu, R. H. Fang, B. T. Luk and L. F. Zhang, *Nanoscale*, 2014, **6**, 65-75.
25. A. Z. Wang, R. Langer and O. C. Farokhzad, *Annu. Rev. Med.*, 2012, **63**, 185-198.
26. J. Gao and B. Xu, *Nano today*, 2009, **4**, 37-51.
27. M.-P. Chien, M. P. Thompson and N. C. Gianneschi, *Chem. Commun.*, 2011, **47**, 167.
28. C. M. Dawidczyk, C. Kim, J. H. Park, L. M. Russell, K. H. Lee, M. G. Pomper and P. C. Searson, *Journal of controlled release : official journal of the Controlled Release Society*, 2014, **187**, 133-144.
29. J. Xie, S. Lee and X. Y. Chen, *Advanced Drug Delivery Reviews*, 2010, **62**, 1064-1079.
30. L. E. Jennings and N. J. Long, *Chem. Commun.*, 2009, 3511-3524.
31. S. Lee and X. Chen, *Molecular Imaging*, 2009, **8**, 87-100.
32. K. Brindle, *Nat. Rev. Cancer*, 2008, **8**, 94-107.
33. S. R. Banerjee, M. Pullambhatla, Y. Byun, S. Nimmagadda, C. A. Foss, G. Green, J. J. Fox, S. E. Lupold, R. C. Mease and M. G. Pomper, *Angew. Chem. Int. Ed.*, 2011, **50**, 9167-9170.
34. E. S. Olson, T. Jiang, T. A. Aguilera, Q. T. Nguyen, L. G. Ellies, M. Scadeng and R. Y. Tsien, *Proc. Natl. Acad. Sci.*, 2010, **107**, 4311-4316.
35. M. A. Whitney, J. L. Crisp, L. T. Nguyen, B. Friedman, L. A. Gross, P. Steinbach, R. Y. Tsien and Q. T. Nguyen, *Nat. Biotech.*, 2011, 1-7.
36. J. F. Desreux, *Inorg. Chem.*, 1980, **19**, 1319-1324.
37. D. Meyer, M. Schaefer and B. Bonnemain, *Invest. Radiol.*, 1988, **23**, S232-S235.
38. J. N. Israelachvili, *Intermolecular and Surface Forces*, Academic Press 2011.
39. S. Futaki, W. Ohashi, T. Suzuki, M. Niwa, S. Tanaka, K. Ueda, H. Harashima and Y. Sugiura, *Bioconjug. Chem.*, 2001, **12**, 1005-1011.
40. I. A. Khalil, S. Futaki, M. Niwa, Y. Baba, N. Kaji, H. Kamiya and H. Harashima, *Gene Ther.*, 2004, **11**, 636-644.
41. Z. P. Chen, P. C. Zhang, A. G. Cheetham, J. H. Moon, J. W. Moxley, Y. A. Lin and H. G. Cui, *Journal of Controlled Release*, 2014, **191**, 123-130.

Journal Name

42. P. C. Zhang, L. L. Lock, A. G. Cheetham and H. G. Cui, *Molecular Pharmaceutics*, 2014, **11**, 964-973.
43. V. Vichai and K. Kirtikara, *Nature protocols*, 2006, **1**, 1112-1116.
44. P. Caravan, J. J. Ellison, T. J. McMurry and R. B. Lauffer, *Chem. Rev.*, 1999, **99**, 2293-2352.
45. G. M. Nicolle, E. Toth, K.-P. Eisenwiener, H. R. Macke and A. E. Merbach, *J. Biol. Inorg. Chem.*, 2002, **7**, 757-769.
46. S. Bull, M. Guler, R. Bras, T. Meade and S. Stupp, *Nano Lett.*, 2005, **5**, 1-4.
47. P. Caravan, C. T. Farrar, L. Frullano and R. Uppal, *Contrast Media Mol. Imaging*, 2009, **4**, 89-100.
48. A. Ghosh, M. Haverick, K. Stump, X. Yang, M. F. Tweedle and J. E. Goldberger, *J. Am. Chem. Soc.*, 2012, **134**, 3647-3650.